

# A Method for Establishing the Handedness of Biological Macromolecules

David M. Belnap,<sup>1</sup> Norman H. Olson, and Timothy S. Baker<sup>2</sup>

*Department of Biological Sciences, Purdue University, West Lafayette, Indiana 47907-1392*

Received August 7, 1996, and in revised form June 10, 1997

**When biological macromolecules are imaged in the transmission electron microscope (TEM), their inherent handedness is lost because the three-dimensional (3D) structure is projected onto a two-dimensional (2D) plane, and identical 2D projections can be made from either 3D enantiomer. Nevertheless, tilt experiments in the TEM can be used to determine handedness. These experiments have been performed successfully on negatively stained specimens. More recently, the method was applied to unstained, frozen-hydrated specimens imaged by means of cryoelectron microscopy (cryo-TEM) methods. Tilt experiments involve recording two micrographs of the same particles at different tilt angles, computing enantiomeric reconstructions from particle images in one micrograph, predicting orientations of corresponding particles in the second micrograph, and comparing model projections with particle images in the second micrograph. In principle, this procedure can be used to determine the handedness of any biological macromolecule imaged by cryoTEM, provided the enantiomeric reconstructions are distinguishable.** © 1997

Academic Press

## INTRODUCTION

Biological macromolecules are enantiomeric because they are made of chiral components such as amino acid residues. Images recorded in a transmission electron microscope (TEM)<sup>3</sup> approximate two-dimensional (2D) projected views of the three-dimensional (3D) objects placed in the specimen holder. The 3D structure of an object can be recon-

structed from projection images by a variety of image processing techniques (e.g., Amos *et al.*, 1982; Frank, 1996; Fuller *et al.*, 1996; Morgan *et al.*, 1995). However, information which defines the *absolute* hand of a macromolecule is lost in a TEM image, and hence in any subsequent 3D reconstruction, because identical 2D projections can be formed from either member of an enantiomeric pair.

The absolute hand of a structure can be determined by use of a tilt experiment. The basic principles in determining handedness by this method are illustrated with models of left and right human hands (Fig. 1). The projected image of a left hand, facing palm down and with the small finger bent toward the palm, is indistinguishable from the projected image of a right hand, facing palm up and with the small finger bent toward the palm (Fig. 1, top and middle rows). However, when each hand is rotated 45° about a vertical axis, the projected images become distinguishable (Fig. 1, top and bottom rows).

Tilt experiments have been used to determine the handedness of biological macromolecules imaged by TEM (e.g., Klug and Finch, 1968; Compans *et al.*, 1972; Finch, 1972, 1974; Linck and Amos, 1974; Nonomura and Kohama, 1974; Cheng *et al.*, 1995; Chrétien *et al.*, 1996; Shaw *et al.*, 1996). We recently determined the hand of three papillomavirus capsids by means of tilting experiments (Belnap *et al.*, 1996). Essential aspects of the Klug and Finch (1968) procedure were adapted for our experiments. They compared projections of computer-generated models to images of negatively stained viruses. We compared projections of 3D reconstructions to images of unstained, frozen-hydrated specimens (cryoTEM images). We used simian virus 40 (SV40), a polyomavirus whose handedness was previously established by electron microscopy (Anderer *et al.*, 1967) and X-ray crystallography (Liddington *et al.*, 1991), as a control in establishing a self-consistent set of conventions in our microscope and image processing procedures.

Papillomavirus capsids are composed of 72 capsomeres arranged on an icosahedral lattice that has a triangulation number of seven ( $T = 7$ ) (see Belnap *et*

<sup>1</sup> Current address: Building 6, Room B2-34, National Institutes of Health, Bethesda, Maryland 20892-2717.

<sup>2</sup> To whom correspondence should be addressed. Fax: 765-496-1189. E-mail: tsb@bragg.bio.purdue.edu.

<sup>3</sup> Abbreviations used: 2D, two-dimensional; 3D, three-dimensional; CC, correlation coefficient; cryoTEM, transmission electron microscopy of unstained, frozen-hydrated specimens; *d*, dextro; *l*, laevo; SV40, simian virus 40; *T*, triangulation number;  $T = 7$ , triangulation number of seven; TEM, transmission electron microscope (or transmission electron microscopy).

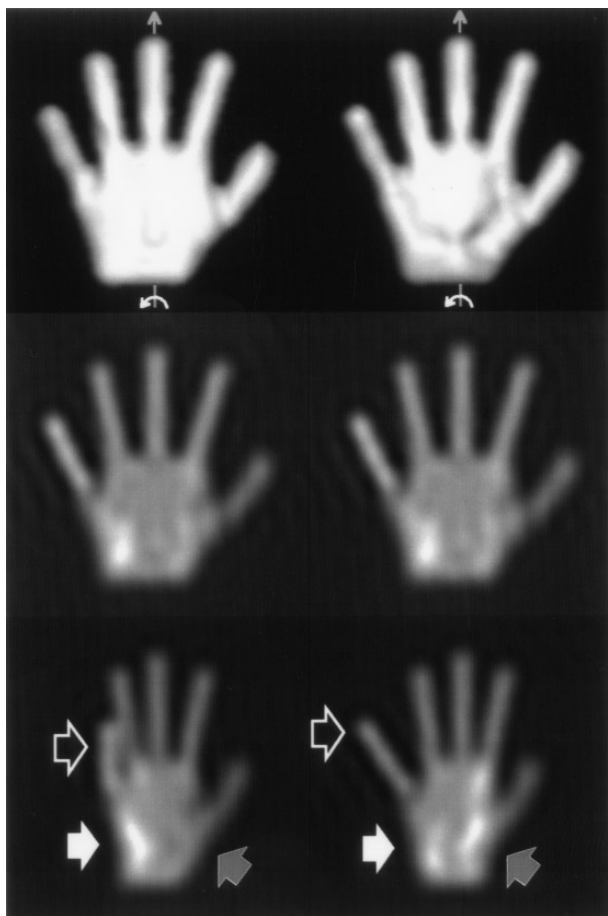


**FIG. 1.** Specimen tilts provide handedness information. (Top row) Surface-shaded views of computer-generated, 3D (“boneless”) models of a left hand with the palm down (left) and a right hand with the palm up (right). In each model, the small finger is bent slightly toward the palm. (Middle row) Projected images of the 3D models in the same orientation as shown in the top row. The projections are identical. Hence, enantiomers cannot be distinguished from these images alone. Projections of 3D objects, such as those recorded by transmission electron microscopy and those in the middle and bottom rows, are analogous to X-ray images of body parts. A projected intensity value is the summation of all object densities along the view direction. Consequently, the X-ray images of a human left hand, palm down, and a right hand, palm up, are similar. (Bottom row) Projected images of the 3D models (top row) after each model was tilted 45° counterclockwise about a vertical axis, as viewed from each wrist (arrows, top row). Each projection exhibits different features, so the enantiomers can be distinguished. Arrows identify some significant differences.

The orientation of the hands in this example was chosen because of convenience and to make it easy for you to try with your own hands. It is important to note that any orientation of a left or right hand could have been chosen. Its projection could be copied by first inverting the 3D model ( $\rho_2[x, y, z] = \rho_1[-x, -y, -z]$ ), second rotating it 180° (in the plane of view), and third projecting it.

*al.*, 1996). The  $T = 7$  lattice, a geometric construct, has defined left-handed ( $T = 7$  *laevo*) and right-handed ( $T = 7$  *dextro*) forms. The  $T = 7$  lattice hand in papillomaviruses is connected to handedness at all structural levels—from the L-amino acids that

make up the polypeptide chain to the quaternary interactions that form the capsid complex (see also Milton *et al.*, 1992).

Handedness was a critical issue in the Belnap *et al.* (1996) study for two reasons. First, the lattice hand for two papillomavirus capsids was reported previously to be different (Finch and Klug, 1965; Klug and Finch, 1965, 1968; Yabe *et al.*, 1979). Second, the proteins that comprise these capsids have strong sequence identities ( $\geq 48\%$ ) and, when displayed with the same lattice hand, similar quaternary structures (Belnap *et al.*, 1996). It is widely held that protein domains adopt the same fold structure if their sequences have  $>30\%$  identity (Orengo *et al.*, 1994). If the lattice hand difference was real, it would be a significant deviation from the observed rule. The lattice hands of all papillomaviruses examined were found to be  $T = 7$  *dextro* (Belnap *et al.*, 1996), by the method outlined below.

## METHOD

The general scheme for the hand determination of papillomavirus  $T = 7$  lattices is depicted in Fig. 2. It involves recording two micrographs of the same particles at different tilt angles, computing enantiomeric reconstructions from particle images in one micrograph, predicting orientations of corresponding particles in the second micrograph, and comparing model projections with particle images in the second micrograph. A similar strategy could be employed to determine the handedness of any biological macromolecule.

### Record Tilt Pair

Two micrographs of the same field of particles are recorded under identical conditions (e.g., magnification, voltage, and so forth) at approximately the same defocus level, with a consistent set of conventions (Table I) but at different tilt angles,  $\beta_1$  and  $\beta_2$ . The  $\beta$  value, which is read directly from the microscope goniometer, specifies the angle by which the specimen is rotated around the microscope tilt axis. In our study, the first image in each pair was taken with untilted samples ( $\beta_1 = 0^\circ$ ) and the second with samples tilted by  $-5^\circ$  ( $\beta_2 = -5^\circ$ ) (Belnap *et al.*, 1996). The two views can be recorded with any choice of  $\beta_1$  and  $\beta_2$  as long as the difference in angle,  $\beta_2 - \beta_1$  or  $\Delta\beta$ , is large enough to provide distinguishable projection images of the object. In a 60-nm spherical object, a  $5^\circ$  tilt shifts surface features on opposite sides of the object by 5.2 nm. This is sufficient to produce unique views of papillomaviruses in images recorded at moderate ( $\leq 3\text{--}5$  nm) or higher resolutions.

The tilt axis of an electron microscope is fixed and coincides with the long axis of the specimen holder rod. However, because the rotational orientation of an electron image depends on excitations of the imaging electromagnetic lenses and hence varies with magnification, the direction of the tilt axis ( $\alpha$ ) also varies and must be accurately determined for each magnification setting used on a given microscope. We define  $\alpha$  as the angle between the long axis of the micrograph and the projection of the tilt axis onto the micrograph, measured positive in a clockwise direction as shown (Fig. 2).

We determined  $\alpha$  by first recording micrographs of a holey-carbon film with the specimen tilted  $\geq 20^\circ$  and with the center of view in focus. The tilt axis was identified as the line dividing the underfocus and overfocus regions of the image. A second method for finding  $\alpha$  involves recording a double exposure, with the specimen translated to two positions along the tilt axis. The axis is

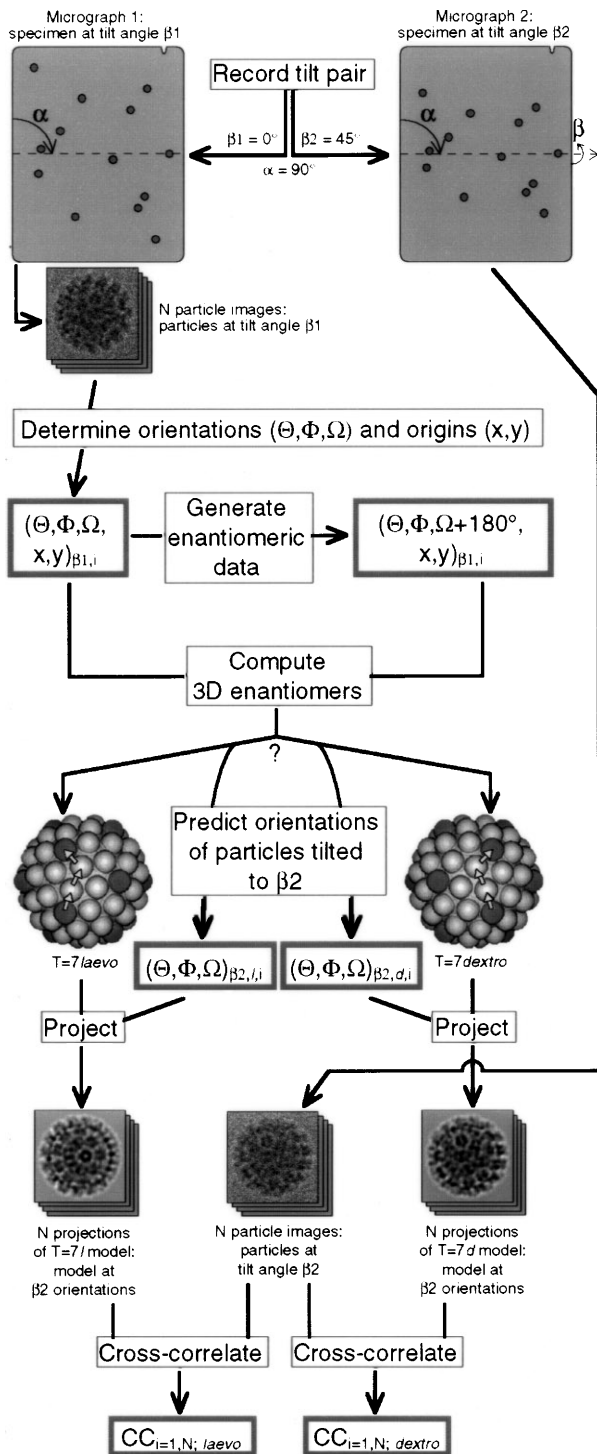


**FIG. 2.** Procedure for determining the handedness of a biological macromolecule. Our convention for viewing the micrographs was to place them with the notch in the upper righthand corner. The curved arrow labeled  $\beta$  indicates a clockwise rotation of the specimen by  $\beta$  degrees about the tilt axis (dashed line), as viewed from the right. The angle  $\alpha$  is the tilt axis direction. The  $\beta_2$ - $\beta_1$  angle ( $45^\circ$ ) is exaggerated here relative to typical experimental conditions to emphasize foreshortening effects. We used a  $-5^\circ$  angle in our experiments with papillomaviruses (Belnap *et al.*, 1996). Abbreviations: CC, correlation coefficient; *l*, laevo; *d*, dextro.

**TABLE I**  
Conventions for Tilt Experiments

Convention	Essential?
(1) Apply sample to same side of grid	No
(2) Place grid in microscope holder with same side facing electron source <sup>a</sup>	No
(3) Orient photographic film consistently with respect to viewing screen, camera holder, and electron source	Yes
(4) Record images of standard and sample at same magnification and voltage to define $\alpha$ and sign of $\Delta\beta$	Yes
(5) Record images at same defocus level	No
(6) Rotate specimen by the same angle	No
(7) Orient micrographs consistently in digital scanning device	Yes
(8) Keep images in the same view direction when displaying, storing, extracting, and manipulating in the computer	Yes

*Note.* Conventions used to record two images of the same field of view and analyze them by computer image processing are listed. Steps that must be performed in a consistent manner are identified. Data from hand determination experiments will not be reliable if these steps are not performed in a consistent fashion. In practice, most successful microscopy is a result of strict adherence to a set of consistent and well-tested procedures. In the list it is assumed that  $\alpha$  and the sign convention of  $\Delta\beta$  are known from calibration with a standard.

<sup>a</sup> As obvious as this may seem, both images in a tilt pair must be recorded before the specimen is removed from the microscope.

parallel to each line connecting any two identical points. Also, image foreshortening that occurs upon tilting from  $0^\circ$  to  $\beta$  can be used to determine both  $\alpha$  and  $\beta$ . The direction of maximum foreshortening occurs perpendicular to the tilt axis and the magnitude of foreshortening is proportional to  $\cos(\beta)$ .

Once  $\alpha$  is known the tilt axis can be drawn as a straight line across a micrograph (e.g., see Fig. 2b in Belnap *et al.*, 1996). There are two possible choices for  $\alpha$ , differing by  $180^\circ$ . The sign of  $\Delta\beta$  depends on this choice. Hence, we recommend the use of control samples (e.g., SV40) for hand determination experiments. Such a standard establishes a consistent set of conventions not only for  $\alpha$  and the sign of  $\Delta\beta$  but for other important steps such as placement of the micrograph in the scanning device (Table I). If the established protocol is followed exactly (Table I), the control sample is no longer required for future experiments.

#### Determine $\beta_1$ Orientations and Origins

We determined origins and orientations for all  $\beta_1$  particles  $(\Theta, \Phi, \Omega, x, y)_{\beta_1=0^\circ, i=1, N}$  as described (Belnap *et al.*, 1996). The  $x, y$  origin of each particle identifies the center of the particle within each image. The angles  $\Theta, \Phi$ , and  $\Omega$  describe each particle's orientation with reference to a fixed  $xyz$  coordinate frame (Fig. 3a).

Virus particles usually lie in random orientations on the microscope grid. Each particle's orientation is specified by the spherical coordinates  $\Theta, \Phi$ , and  $\Omega$ , which are analogous to latitude, longitude, and compass bearing, respectively, used in navigation (Fig. 3a). For example, if for the left hand in Fig. 1 (top row, left) we define the arrow as the  $z$ -axis with the  $x$ -axis towards the viewer and the  $y$ -axis directed to the right in the plane of the hand, then the left hand is viewed in the orientation  $(90^\circ, 0^\circ, 0^\circ)$ . If, for the right hand positioned as shown (Fig. 1, top row, right), the  $x$ -axis remains towards the viewer but the  $y$  and  $z$  axes are rotated by  $180^\circ$  about  $x$ , then the orientation of the right hand is  $(90^\circ, 0^\circ, 180^\circ)$ .



computed by the inversion operation [Eq. (1)]. Though the handedness of each enantiomer is fixed by the choice of orientation ( $\Omega$  or  $\Omega + 180^\circ$ ), it remains unknown until each reconstruction is viewed. This hand ambiguity arises because the image analysis procedures fix the hand to correlate with an arbitrarily chosen reference particle of unknown handedness [e.g., cross-common-lines method (Fuller *et al.*, 1996)] or with a chosen model of known handedness [e.g., polar-Fourier-transform routine (Baker and Cheng, 1996)]. At this point, the correct enantiomer is still unknown, though it is known which enantiomer corresponds to  $\Omega_{\beta 1}$  and which corresponds to  $(\Omega + 180^\circ)_{\beta 1}$ .

#### *Predict Orientations of Particles Tilted to $\beta 2$*

Predicted sets of orientations for each enantiomer ( $\beta 2$  view) are calculated by applying the appropriate rotational transformation (a rotation of  $\Delta\beta$  about axis direction  $\alpha$ ) to the  $(\Theta, \Phi, \Omega)_{\beta 1, i}$  and  $(\Theta, \Phi, \Omega + 180^\circ)_{\beta 1, i}$  orientations. We used spherical trigonometry and assumed the rotation from  $\beta 1$  to  $\beta 2$  followed the path of a great circle (Appendix, Fig. 3). This method is comparable to navigation where one knows the starting position  $(\Theta, \Phi)_{\beta 1}$ , initial course  $(\Theta_{\beta 1} + \alpha + 90^\circ)$ , and distance to be traveled ( $\Delta\beta$ ) but does not know the final destination  $(\Theta, \Phi)_{\beta 2}$  (e.g., Kells *et al.*, 1942; Gellert *et al.*, 1977).

The direction of the  $\beta 1$ -to- $\beta 2$  rotation is  $180^\circ$  different for  $(\Theta, \Phi, \Omega)_{\beta 1}$  compared to  $(\Theta, \Phi, \Omega + 180^\circ)_{\beta 1}$  (Fig. 3c). Hence, each pair of  $(\Theta, \Phi, \Omega)_{\beta 2, \text{laevo}, i}$  and  $(\Theta, \Phi, \Omega)_{\beta 2, \text{dextro}, i}$  values represent distinct orientations. For example, if the left and right hands in Fig. 1 (top row) have the orientations  $(90^\circ, 0^\circ, 0^\circ)$  and  $(90^\circ, 0^\circ, 180^\circ)$ , respectively, the tilt axis is coincident with the  $+z$  axis for the left hand and the  $-z$  axis for the right hand. After rotating the hands by  $45^\circ$  as shown (Fig. 1, top row) the left hand is at  $(90^\circ, 45^\circ, 0^\circ)$  and the right hand at  $(90^\circ, -45^\circ, 180^\circ)$ . The untilted particle in Fig. 2 has  $(\Theta, \Phi, \Omega)_{\beta 1}$  equal to  $(80^\circ, -11^\circ, 59^\circ)$  which corresponds to a  $T = 7I$  structure and  $(\Theta, \Phi, \Omega + 180^\circ)_{\beta 1} = (80^\circ, -11^\circ, 239^\circ)$  for a  $T = 7d$  structure. A  $45^\circ$  rotation about a tilt axis with  $\alpha = 90^\circ$  transforms these two orientations into  $(\Theta, \Phi, \Omega)_{\beta 2, l} = (103.6^\circ, -49.6^\circ, 60.3^\circ)$  and  $(\Theta, \Phi, \Omega)_{\beta 2, d} = (61.2^\circ, 32.8^\circ, 254.4^\circ)$ .

In general,  $\Omega_{\beta 2, l, i}$  and  $\Omega_{\beta 2, d, i}$  are not related by a  $180^\circ$  rotation, and the two  $\beta 2$  views corresponding to each pair (computed in the next step) are not mirror images of each other (see Fig. 2). One exception, for example as in the previous paragraph for the left and right hands, is if a particle has a  $\beta 1$  orientation with  $\Theta = 90^\circ$ . In this case, the resulting  $\Omega_{\beta 2, l}$  and  $\Omega_{\beta 2, d}$  angles are related by  $180^\circ$ , though the  $(\Theta, \Phi)_{\beta 2}$  positions differ. (If the object has icosahedral symmetry, the resulting projections are also related by a  $180^\circ$  rotation.)

#### *Project 3D Enantiomers along $\beta 2$ Orientations*

The two orientations just calculated for each particle specify how each enantiomer is to be rotated into the appropriate view direction. Once rotated to the predicted  $\beta 2$  orientation, each 3D model is projected and, in the next step, compared to the experimental ( $\beta 2$ ) image. The two projections are different because they arise from enantiomers at distinct orientations. Only one of the two will match the  $\beta 2$  image.

#### *Cross-Correlate Projections of Enantiomeric Models with $\beta 2$ Images*

Projections of the two enantiomers are cross-correlated (Dryden *et al.*, 1993) with the corresponding images of the particles at tilt angle  $\beta 2$ . The set of projections which best matches the images of particles at tilt angle  $\beta 2$  identifies the correct enantiomer. Such quantitative analysis of noisy cryoTEM data is more reliable than simple visual comparisons (see Belnap *et al.*, 1996).

The reliability of the cross-correlation analysis can be improved by means of real-space and reciprocal-space (resolution) filtering operations. For SV40 and the three papillomaviruses, we used all

intensities within each particle, and we filtered data to include spatial frequencies between approximately  $\frac{1}{16}$  and  $\frac{1}{3.7}$  nm<sup>-1</sup>. All projections of the  $T = 7d$  enantiomer correlated much better with the  $\beta 2$  images than did projections of the  $T = 7I$  enantiomer (Belnap *et al.*, 1996).

## DISCUSSION

For TEM imaging at 2 to 3 nm resolution, the depth of field ( $>200$  nm) far exceeds the dimensions of most biological specimens. Hence, micrographs are regarded as 2D projections of the 3D specimens.

Regardless of an object's orientation, it is impossible to determine its absolute hand from a single projection image (Fig. 1, middle row). Any set of particle images will yield enantiomeric reconstructions if both sets of orientation and origin parameters,  $(\Theta, \Phi, \Omega, x, y)$  and  $(\Theta, \Phi, \Omega + 180^\circ, x, y)$ , are assigned to the image data. A second view is required in which the specimen is tilted by a specified angle about a defined axis. The second view will be consistent with only one enantiomer in both appearance (Fig. 1, bottom row) and  $\Theta, \Phi, \Omega$  orientation.

Three-dimensional models or reconstructions provide sufficient information to determine the handedness of a structure by means of tilting experiments (see also Klug and Finch, 1968; Finch, 1972). It is not necessary to initially know the correct hand because the 3D model can be inverted Eq. (1) and then projected to simulate the second view.

Viewing the 3D structure is advantageous in defining the correct enantiomer and essential in properly interpreting the structure. But, in theory, it is not necessary to compute 3D reconstructions and 2D projections to determine which set of orientations,  $(\Theta, \Phi, \Omega)_{\beta 1}$  or  $(\Theta, \Phi, \Omega + 180^\circ)_{\beta 1}$ , represents the correct hand. Orientations for both sets of particle images could be found by common lines methods (Fuller *et al.*, 1996). Predicted orientations could be computed from  $(\Theta, \Phi, \Omega)_{\beta 1}$  and  $(\Theta, \Phi, \Omega + 180^\circ)_{\beta 1}$  and compared to the measured orientations of the  $\beta 2$  particles. Indeed, we successfully applied this approach to our SV40 image data and found that the predicted  $T = 7d$  orientations compared much better to the measured orientations of  $\beta 2$  particles than did the predicted  $T = 7I$  orientations. In practice, however, 3D reconstructions and 2D projections are relatively easy to compute once a set of orientations is available and usually are computed as part of a refinement process. In addition, the 3D and 2D data are powerful tools with which to judge the reliability of the measured orientations. Therefore, this alternative method merely supplements the described procedure (Fig. 2).

#### *Practical Applications*

In principle, the method we describe (Fig. 2) can be used with any biological macromolecule imaged by

cryoTEM. A skewed lattice like the papillomavirus  $T = 7$  lattice and prominent features like the papillomavirus capsomeres together provide strong, low-resolution features which make it relatively easy to distinguish handedness by this technique. A similar procedure was used to demonstrate that the skewed lattice of aquareovirus ( $T = 13$ ) was *laevo* (Shaw *et al.*, 1996).

The strong, low-resolution features of papillomaviruses also made it possible to determine the lattice hand of the  $T = 7$  capsid by use of a metal-shadowing technique (Belnap *et al.*, 1996) and by use of tilt experiments with negatively stained specimens (Klug and Finch, 1968). However, the handedness of most biological macromolecules is a more subtle feature that is obscured by metal shadowing or negative staining procedures.

CryoTEM has important advantages over other conventional EM methods (see, for example, Adrian *et al.*, 1984, and Stewart and Vigers, 1986, for reviews). Staining or shadowing techniques dehydrate the sample and embed it in metal. Both of these effects may alter the specimen's appearance and size (e.g., Earnshaw *et al.*, 1978). CryoTEM provides a way to preserve the native, or near-native, hydrated state under high vacuum. Some highly ordered, crystalline specimens have been preserved to atomic resolution by cryoTEM (e.g., Taylor and Glaeser, 1974; Kühlbrandt *et al.*, 1994). In addition, it is mainly low-resolution, surface features that are observed with techniques such as negative staining and metal shadowing. CryoTEM and 3D image reconstruction allow both external and internal features to be seen at higher resolution. Our experiments with papillomaviruses and SV40 (Belnap *et al.*, 1996) and experiments by others (Prasad *et al.*, 1992; Cheng *et al.*, 1995; Chrétien *et al.*, 1996; Shaw *et al.*, 1996) show that the tilting experiment first outlined by Klug and Finch (1968) with negatively stained samples also is effective with images recorded by cryoTEM techniques.

The subtle handedness of features in other macromolecules, including icosahedral viruses with non-skewed lattices (e.g.,  $T = 4$  and  $T = 16$ ), could be determined from cryoTEM images by the method reported here. For example, the correct hand of the  $T = 4$  Ross River virus was readily determined because the flower-like, trimeric, glycoprotein spikes on the viral surface are strong, chiral features (Cheng *et al.*, 1995). For features with even more subtle chirality, such as the capsomeres of  $T = 16$  herpes simplex virus (Booy *et al.*, 1991) or of the  $T = 25$  adenovirus (Stewart *et al.*, 1991), hand determination is more difficult and requires analysis at a resolution high enough to detect chirality. Note that

it is only necessary to detect chiral features in reconstructions computed from the first image set, provided  $\Delta\beta$  is large enough to produce distinct views of particles in both micrographs. The same resolution in the second image set, which in practice is difficult to achieve owing to irradiation effects, is unnecessary because changes in orientation usually can be detected at resolutions much lower than those required to reveal chiral structural features. Indeed, differences in the  $\beta_1$  and  $\beta_2$  views of a particle often are detectable by eye (see Figs. 2 and 4 in Belnap *et al.*, 1996).

We thank R. A. Crowther for help in clarifying the relationship of enantiomers to their resulting projection images, E. Kocsis for helpful suggestions on the manuscript, and P. Penczek for help in understanding conventions of orientation angles. This work was supported by U.S. Public Health Service Grant GM33050 (T.S.B.), by a grant from the Lucille P. Markey Charitable Trust for Structural Biology (Purdue University), and by a National Institutes of Health Training Grant (D.M.B.).

## REFERENCES

- Adrian, M., Dubochet, J., Lepault, J., and McDowell, A. W. (1984) Cryo-electron microscopy of viruses, *Nature* **308**, 32–36.
- Amos, L. A., Henderson, R., and Unwin, P. N. T. (1982) Three-dimensional structure determination by electron microscopy of two-dimensional crystals, *Prog. Biophys. Mol. Biol.* **39**, 183–231.
- Anderer, F. A., Schlumberger, H. D., Koch, M. A., Frank, H., and Eggers, H. J. (1967) Structure of simian virus 40: II. Symmetry and components of the virus particle, *Virology* **32**, 511–523.
- Baker, T. S., and Cheng, R. H. (1996) A model-based approach for determining orientations of biological macromolecules imaged by cryoelectron microscopy, *J. Struct. Biol.* **116**, 120–130.
- Belnap, D. M., Olson, N. H., Cladel, N. M., Newcomb, W. W., Brown, J. C., Kreider, J. W., Christensen, N. D., and Baker, T. S. (1996) Conserved features in papillomavirus and polyomavirus capsids, *J. Mol. Biol.* **259**, 249–263.
- Booy, F. P., Newcomb, W. W., Trus, B. L., Brown, J. C., Baker, T. S., and Steven, A. C. (1991) Liquid-crystalline, phage-like packing of encapsidated DNA in herpes simplex virus, *Cell* **64**, 1007–1015.
- Cheng, R. H., Kuhn, R. J., Olson, N. H., Rossmann, M. G., Choi, H., Smith, T. J., and Baker, T. S. (1995) Nucleocapsid and glycoprotein organization in an enveloped virus, *Cell* **80**, 621–630.
- Chrétien, D., Kenney, J. M., Fuller, S. D., and Wade, R. H. (1996) Determination of microtubule polarity by cryo-electron microscopy, *Structure* **4**, 1031–1040.
- Compans, R. W., Mountcastle, W. E., and Choppin, P. W. (1972) The sense of the helix of paramyxovirus nucleocapsids, *J. Mol. Biol.* **65**, 167–169.
- Dryden, K. A., Wang, G., Yeager, M., Nibert, M. L., Coombs, K. M., Furlong, D. B., Fields, B. N., and Baker, T. S. (1993) Early steps in reovirus infection are associated with dramatic changes in supramolecular structure and protein conformation: Analysis of virions and subviral particles by cryoelectron microscopy and image reconstruction. *J. Cell Biol.* **122**, 1023–1041.
- Earnshaw, W. C., King, J., and Eiserling, F. A. (1978) The size of the bacteriophage T4 head in solution with comments about the dimension of virus particles as visualized by electron microscopy, *J. Mol. Biol.* **122**, 247–253.

- Finch, J. T. (1972) The hand of the helix of tobacco mosaic virus, *J. Mol. Biol.* **66**, 291–294.
- Finch, J. T. (1974) The surface structure of polyoma virus, *J. Gen. Virol.* **24**, 359–364.
- Finch, J. T., and Klug, A. (1965) The structure of viruses of the papilloma-polyoma type: III. Structure of rabbit papilloma virus, *J. Mol. Biol.* **13**, 1–12.
- Frank, J. (1996) *Three-Dimensional Electron Microscopy of Macromolecular Assemblies*, Academic Press, San Diego.
- Fuller, S. D., Butcher, S. J., Cheng, R. H., and Baker, T. S. (1996) Three-dimensional reconstruction of icosahedral particles—the uncommon line, *J. Struct. Biol.* **116**, 48–55.
- Gellert, W., Küstner, H., Hellwich, M., and Kästner, H. (Eds.) (1977) *The VNR Concise Encyclopedia of Mathematics*, pp. 261–282, Van Nostrand Reinhold, New York.
- Kells, L. M., Kern, W. F., and Bland, J. R. (1942) *Spherical Trigonometry with Naval and Military Applications*, McGraw-Hill, New York.
- Klug, A., and Finch, J. T. (1965) Structure of viruses of the papilloma-polyoma type: I. Human wart virus, *J. Mol. Biol.* **11**, 403–423.
- Klug, A., and Finch, J. T. (1968) Structure of viruses of the papilloma-polyoma type: IV. Analysis of tilting experiments in the electron microscope, *J. Mol. Biol.* **31**, 1–12.
- Kühlbrandt, W., Wang, D. N., and Fujiyoshi, Y. (1994) Atomic model of plant light-harvesting complex by electron crystallography, *Nature* **367**, 614–621.
- Liddington, R. C., Yan, Y., Moulai, J., Sahli, R., Benjamin, T. L., and Harrison, S. C. (1991) Structure of simian virus 40 at 3.8-Å resolution, *Nature* **354**, 278–284.
- Linck, R. W., and Amos, L. A. (1974) The hands of helical lattices in flagellar doublet microtubules, *J. Cell Sci.* **14**, 551–559.
- Milton, R. C. deL., Milton, S. C. F., and Kent, S. B. H. (1992) Total chemical synthesis of a D-enzyme: The enantiomers of HIV-1 protease show demonstration of reciprocal chiral substrate specificity, *Science* **256**, 1445–1448, **257**, 147.
- Morgan, D. G., Owen, C., Melanson, L. A., and DeRosier, D. J. (1995) Structure of bacterial flagellar filaments at 11 Å resolution: Packing of the  $\alpha$ -helices, *J. Mol. Biol.* **249**, 88–110.
- Nonomura, Y., and Kohama, K. (1974) Determination of the absolute hand of the helix in the nucleocapsid of haemagglutinating virus (Japan), *J. Mol. Biol.* **86**, 621–626.
- Orengo, C. A., Jones, D. T., and Thornton, J. M. (1994) Protein superfamilies and domain superfolds, *Nature* **372**, 631–634.
- Prasad, B. V. V., Yamaguchi, S., and Roy, P. (1992) Three-dimensional structure of single-shelled bluetongue virus, *J. Virol.* **66**, 2135–2142.
- Shaw, A. L., Samal, S. K., Subramanian, K., and Prasad, B. V. (1996) The structure of aquareovirus shows how the different geometries of the two layers of the capsid are reconciled to provide symmetrical interactions and stabilization, *Structure* **4**, 957–967.
- Stewart, M., and Vigers, G. (1986) Electron microscopy of frozen-hydrated biological material, *Nature* **319**, 631–636.
- Stewart, P. L., Burnett, R. M., Cyrklaff, M., and Fuller, S. D. (1991) Image reconstruction reveals the complex molecular organization of adenovirus, *Cell* **67**, 145–154.
- Taylor, K. A., and Glaeser, R. M. (1974) Electron diffraction of frozen, hydrated protein crystals, *Science* **186**, 1036–1037.
- Yabe, Y., Sadakane, H., and Isono, H. (1979) Connection between capsomeres in human papilloma virus, *Virology* **96**, 547–552.

## APPENDIX

**Prediction of the  $\beta_2$  Orientation by the Use of Spherical Trigonometry**  
D. M. Belnap

The following method for computing  $(\Theta, \Phi, \Omega)_{\beta_2}$  relies on the described convention for  $\Theta$ ,  $\Phi$ , and  $\Omega$  (Fig. 3a). Other conventions would require a modified procedure.

*Define an Oblique Spherical Triangle*

To solve for  $(\Theta, \Phi, \Omega)_{\beta_2}$  we first define an oblique spherical triangle (Fig. 3b). An oblique spherical triangle has three vertices, sides, and angles. All are described by angular measurements.

The three vertices are at  $\Theta = 0^\circ$ ,  $(\Theta, \Phi)_{\beta_1}$ , and  $(\Theta, \Phi)_{\beta_2}$ .

The three sides are  $\Theta_{\beta_1}$ ,  $\Theta_{\beta_2}$ , and  $\Delta\beta$ . Each is an arc on a great circle. A great circle is the intersection of a sphere with a plane that passes through the center of the sphere. The equator and meridians are examples of great circles on the earth. The shortest distance between any two points on a sphere is the path of a great circle. The tilt axis is perpendicular to the great circle that  $\Delta\beta$  follows. With the tilt axis pointing at the viewer,  $\Delta\beta$  is positive when the rotation of the *object* is clockwise. ( $\Delta\beta$  is positive in Figs. 1, 2, and 3b.)

The three angles are angles between the great circles that intersect at the vertices. One is  $\Delta\Phi$  and equals  $\Phi_{\beta_2} - \Phi_{\beta_1}$ . The other two angles are  $F_{\beta_1}$ , the forward course at  $\beta_1$ , and  $R_{\beta_2}$ , the reverse course at  $\beta_2$ . They are termed “courses” because, as in navigation, they point in the direction of travel, forward (*F*), or opposite the direction of travel, reverse (*R*). *F* and *R* are measured from the  $+Q$  axis. They are  $180^\circ$  different from each other, but the conventions are opposite. With reference to the viewer, positive values are measured clockwise for *F* and counterclockwise for *R*. The relationship between *F* and *R* is

$$F + R = 180^\circ. \quad (2)$$

*F* is given by

$$F = \Omega + \alpha + 90^\circ. \quad (3)$$

By substituting Eq. (3) into Eq. (2) and reducing to lowest terms

$$R = 90^\circ - \Omega - \alpha. \quad (4)$$

*F* and *R* are angles with respect to the *PQ* axes (Figs. 3a and 3c). Hence, in general, values of *F* and *R* change with movement along a great circle. By analogy to navigation, the only exceptions are for east or west travel along the equator (i.e.,  $\Theta$  is

always 90°) or north or south travel along a meridian (i.e., toward +z or -z). Barring these exceptions, the change in  $F$  and  $R$  during tilting means a change in  $\Omega$  since  $\alpha$  is always perpendicular to the direction of rotation. Consequently,

$$F_{\beta 1} = \Omega_{\beta 1} + \alpha + 90^\circ, \quad (5)$$

$$R_{\beta 2} = 90^\circ - \Omega_{\beta 2} - \alpha, \quad (6)$$

$$\Omega_{\beta 2} = 90^\circ - R_{\beta 2} - \alpha. \quad (7)$$

$(\Theta, \Phi, \Omega)_{\beta 2}$  can now be solved from  $\Theta_{\beta 1}$ ,  $\Delta\beta$ , and  $F_{\beta 1}$ .

### Calculate $\beta 2$ Orientation

The following method, which works irrespective of symmetry considerations, can be used to compute  $(\Theta, \Phi, \Omega)_{\beta 2}$  over all  $\Theta, \Phi$ , and  $\Omega$  for  $0^\circ < |\Delta\beta| \leq 90^\circ$ . I have written a computer program that performs these calculations. It is available free upon request.

If  $F_{\beta 1} \neq 0^\circ$  or  $180^\circ$ , the  $\beta 2$  angles can be solved by spherical trigonometry (Selby, 1967). First, find  $\Theta_{\beta 2}$  by the haversine formula

$$\sin^2 \left( \frac{\Theta_{\beta 2}}{2} \right) = \sin^2 \left( \frac{\Theta_{\beta 1} - \Delta\beta}{2} \right) + \sin \Theta_{\beta 1} \sin \Delta\beta \sin^2 \left( \frac{F_{\beta 1}}{2} \right). \quad (8)$$

Next, concurrently solve two Napier's analogies to calculate  $\Delta\Phi$  and  $R_{\beta 2}$

$$\tan \left( \frac{R_{\beta 2} - \Delta\Phi}{2} \right) = \sin \left( \frac{\Theta_{\beta 1} - \Delta\beta}{2} \right) / \tan \left( \frac{F_{\beta 1}}{2} \right) \sin \left( \frac{\Theta_{\beta 1} + \Delta\beta}{2} \right) \quad (9)$$

$$\tan \left( \frac{R_{\beta 2} + \Delta\Phi}{2} \right) = \cos \left( \frac{\Theta_{\beta 1} - \Delta\beta}{2} \right) / \tan \left( \frac{F_{\beta 1}}{2} \right) \cos \left( \frac{\Theta_{\beta 1} + \Delta\beta}{2} \right) \quad (10)$$

Then,  $\Phi_{\beta 2} = \Phi_{\beta 1} + \Delta\Phi$ , and  $\Omega_{\beta 2} = 90^\circ - R_{\beta 2} - \alpha$  [Eq. (7)].

There are two exceptions to the use of eqs. (9) and

(10) when  $F_{\beta 1} \neq 0^\circ$  or  $180^\circ$ . If (1)  $|\Delta\beta| \geq \Theta_{\beta 1}$  and  $\Delta\beta < 0^\circ$  or (2)  $|\Delta\beta| \geq 180^\circ - \Theta_{\beta 1}$  and  $\Delta\beta > 0^\circ$ , then the following two Gauss's formulae are used instead. (Also, in these two cases, the sign of  $F_{\beta 1}$  is changed if  $180^\circ < |F_{\beta 1}| < 360^\circ$ .)

$$\cos \left( \frac{R_{\beta 2} - \Delta\Phi}{2} \right) = \sin \left( \frac{F_{\beta 1}}{2} \right) \sin \left( \frac{\Theta_{\beta 1} + \Delta\beta}{2} \right) / \sin \left( \frac{\Theta_{\beta 2}}{2} \right) \quad (11)$$

$$\cos \left( \frac{R_{\beta 2} + \Delta\Phi}{2} \right) = \sin \left( \frac{F_{\beta 1}}{2} \right) \cos \left( \frac{\Theta_{\beta 1} + \Delta\beta}{2} \right) / \cos \left( \frac{\Theta_{\beta 2}}{2} \right) \quad (12)$$

The use of Eqs. (11) and (12) instead of (9) and (10) is the only difference in the calculations for these two exceptions.

If  $F_{\beta 1}$  equals  $0^\circ$  or  $180^\circ$ , the  $\beta 2$  angles are not solved by Eqs. (8–12). Instead, a beginning value of  $\Theta_{\beta 2}$  is given by

$$\Theta_{\beta 2, \text{beginning}} = \Theta_{\beta 1} - \Delta\beta \cos F_{\beta 1}. \quad (13)$$

The value of  $\Theta_{\beta 2, \text{beginning}}$  determines how  $\Theta_{\beta 2}$ ,  $\Phi_{\beta 2}$ , and  $\Omega_{\beta 2}$  are calculated. There are five possible cases:

- (1) If  $0^\circ < \Theta_{\beta 2, \text{beginning}} < 180^\circ$ , then  $\Theta_{\beta 2} = \Theta_{\beta 2, \text{beginning}}$ ,  $\Phi_{\beta 2} = \Phi_{\beta 1}$ , and  $\Omega_{\beta 2} = \Omega_{\beta 1}$ .
  - (2) If  $\Theta_{\beta 2, \text{beginning}} = 0^\circ$ , then  $\Theta_{\beta 2} = 0^\circ$ ,  $\Phi_{\beta 2} = 0^\circ$ , and  $\Omega_{\beta 2} = \Omega_{\beta 1} - \Phi_{\beta 1}$ .
  - (3) If  $\Theta_{\beta 2, \text{beginning}} = 180^\circ$ , then  $\Theta_{\beta 2} = 180^\circ$ ,  $\Phi_{\beta 2} = 0^\circ$ , and  $\Omega_{\beta 2} = \Omega_{\beta 1} + \Phi_{\beta 1}$ .
  - (4) If  $\Theta_{\beta 2, \text{beginning}} < 0^\circ$ , then  $\Theta_{\beta 2} = |\Theta_{\beta 2, \text{beginning}}|$ ,  $\Phi_{\beta 2} = \Phi_{\beta 1} + 180^\circ$  and  $\Omega_{\beta 2} = \Omega_{\beta 1} + 180^\circ$ .
  - (5) If  $\Theta_{\beta 2, \text{beginning}} > 180^\circ$ , then  $\Theta_{\beta 2} = 360^\circ - \Theta_{\beta 2, \text{beginning}}$ ,  $\Phi_{\beta 2} = \Phi_{\beta 1} + 180^\circ$ , and  $\Omega_{\beta 2} = \Omega_{\beta 1} + 180^\circ$ .
- Formulas for  $\Theta_{\beta 2}$ , in cases 4 and 5, restrict  $\Theta_{\beta 2}$  to the range 0–180°.

### REFERENCE

Selby, S. M. (Ed.) (1967) CRC Standard Mathematical Tables, 15th ed., pp. 162–164, 305, The Chemical Rubber Co., Cleveland, Ohio.